## **CONFERENCE PRE-PRINT**

# EXPERIMENTAL AND NUMERICAL RESEARCH ON HIGHTEMPERATURE SUPERCONDUCTING DEMOUNTABLE JOINTS FOR TOROIDAL FIELD COILS OF TOKAMAKS

Jiang Yuanchao Shaanxi Startorus Fusion Technology Co., Ltd. Shaanxi, China

Email: qinlang@startorus.cn

Tan Yi Department of Engineering Physics, Tsinghua University, Beijing, China

#### Abstract

In conventional tokamak architecture, the integrally constructed toroidal field (TF) coils circumferentially enclose central solenoid (CS) coils. This configuration categorically prevents vacuum vessel replacements without through-wall disassembly of TF coils—a process fraught with excessive downtime and maintenance costs that render such systems impractical for DEMO stage accessibility. To address this critical bottleneck, contemporary initiatives within the nuclear fusion research community have prioritized the development of demountable toroidal field (TF) coil systems, with the principal engineering challenge residing in the comprehensive design optimization and experimental validation of demountable joint interfaces. Our technical approach involves two synergistic innovations:(1) Damage-resistant copper cladding on Rare earth Elements Barium Copper Oxide (REBCO) tapes for cyclic assembly robustness, (2) Solder hierarchy-differentiated joints combining Sn63Pb37-encapsulated HTS strands with In foil interlayers. The devised joints exploit themelt differential between indium (156.6°C) and Sn63Pb37 alloy (183°C), enabling pressure-regulated detachment via melt viscosity modulation. Experimental validation confirms stable contact resistance (<100 n $\Omega$ ·cm²) through thermal mechanical cycles, with Ic@77K, self-field retaining 98% of initial value. This work establishes a critical prerequisite for industrial-scale implementation of demountable TF systems and provides quantitative design criteria for next-generation tokamaks.

# 1. INTRODUCTION

The tokamak, a leading magnetic confinement concept for achieving controlled nuclear fusion, relies on a complex integration of toroidal field (TF) coils and central solenoid (CS) coils to generate and stabilize the plasma. In conventional tokamak architectures, the TF coils are integrally constructed as a continuous toroidal structure that fully encloses the CS coils and vacuum vessel. While this configuration ensures mechanical integrity and electromagnetic performance, it imposes a critical limitation: the vacuum vessel—a component subject to neutron-induced degradation and frequent maintenance—cannot be replaced without disassembling the TF coil system. Such disassembly necessitates cutting through structural components, resulting in prolonged downtime, exorbitant maintenance costs, and cumulative damage to superconducting materials. These constraints render traditional tokamak designs economically and operationally impractical for DEMO-stage reactors, where rapid component replacement and high availability are paramount.

To overcome this bottleneck, recent fusion engineering efforts have focused on developing demountable TF coil systems that enable non-destructive disassembly and reassembly. The principal challenge lies in engineering robust, high-performance demountable joints capable of sustaining extreme thermal, mechanical, and electromagnetic loads while maintaining ultra-low electrical resistance and minimal critical current (Ic) degradation across repeated assembly cycles. Existing solutions, such as bolted joints or soldering-bonded interfaces, suffer from irreversible mechanical wear, resistance instability under cyclic loading, or incompatibility with high-temperature superconductor (HTS) materials.

This work introduces two synergistic innovations to address these limitations. First, we encapsulate the rare-earth barium copper oxide (REBCO) side of HTS tapes with copper strips of equal width using Sn63Pb37 solder. This approach transforms the original superconducting superconducting interface into a copper-copper contact during disassembly, significantly reducing the risk of HTS material degradation during repeated assembly cycles. Second, we propose a hierarchical soldered joint architecture: by integrating the Sn63Pb37-encapsulated REBCO-copper composite from the first innovation, the construction of superconducting joints now only requires connecting the pre-clad copper strips. To achieve this, indium (In) foil is employed as the interfacial medium between copper strips. Leveraging the melting point differential between In (156.6°C) and Sn63Pb37 (183°C), the joints enable

pressure-regulated detachment through selective melting of the In layer, preserving the structural integrity of the REBCO tapes. Experimental validation demonstrates stable contact resistance ( $<85~\text{n}\Omega\cdot\text{cm}^2$ ) over multiple assembly cycles, with Ic@77K, self-field retaining 98% of its initial value—a milestone achievement for HTS-compatible demountable magnet systems.

This study not only resolves a critical engineering barrier for DEMO-reactor maintainability but also establishes quantitative design criteria for joint geometry, solder hierarchy, and operational temperature windows. By bridging the gap between theoretical concepts and industrial-scale feasibility, our work advances the realization of practical, high-availability tokamaks for commercial fusion energy.

## 2. DEMOUNTABLE JOINT DESIGN AND SAMPLE PREPARATION

# 2.1. Joint Structure Design

This study uses YBCO second-generation HTS tapes from Shanghai Superconductor. Key parameters are listed in Table 1. Lap joints are the most commonly used joint type in HTS magnets due to their simple structure and ease of implementation. Therefore, the demountable joint studied here is designed as a lap joint, as shown in Figure 1.

TABLE 1. Performance Parameters of YBCO 2G HTS Tape

Parameter	Value
Tape Width	$12 \text{ mm} \pm 0.1 \text{ mm}$
Total Thickness	$92~\mu m \pm 10~\mu m$
Substrate Thickness	$45~\mu m \pm 1~\mu m$
Copper Plating Thickness	$18~\mu m \pm 2~\mu m$
Critical Current	$550~A\sim780~A$

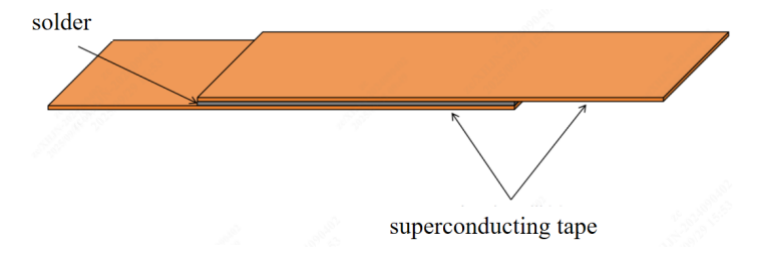


FIG. 1. Schematic diagram of the lap joint structure.

Considering that HTS magnet designs often use multi-tape stacking to reduce induced voltage, this study progresses from single-tape lap joints to nine-tape stacked lap joints, corresponding to the number of tapes used in practical winding configurations (Figure 2).

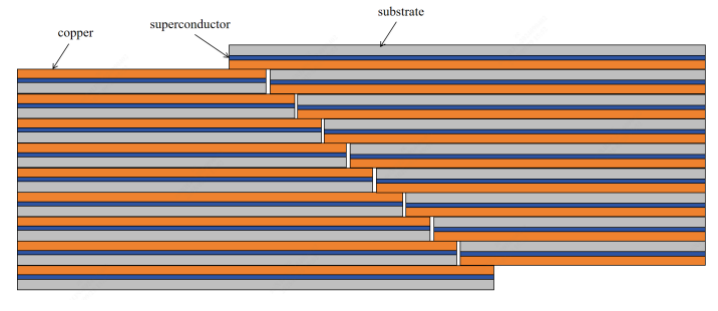


FIG. 2. Schematic diagram of the lap joint structure.

From a material property perspective, YBCO 2G HTS tape has a multi-layer structure (Figure 3). The most vulnerable interface is between the superconducting layer and the silver layer. In HTS magnets, if peeling stress occurs, there is a 90% probability of failure at this interface. The outer electroplated copper layer is very thin (20  $\mu$ m). Considering mechanical strength and solder corrosion, this thin layer cannot adequately protect the internal superconducting layer during repeated joint disassembly. Therefore, we chose to encapsulate an additional 100  $\mu$ m copper strip on the superconducting side of the HTS tape for enhanced protection (Figure 4).

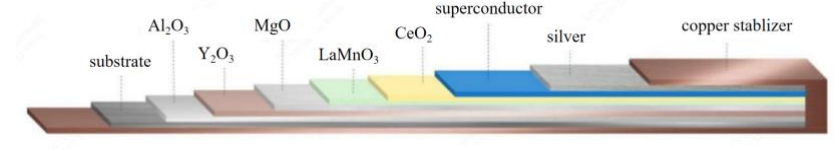


FIG. 3. Schematic diagram of the YBCO high-temperature superconducting tape structure.

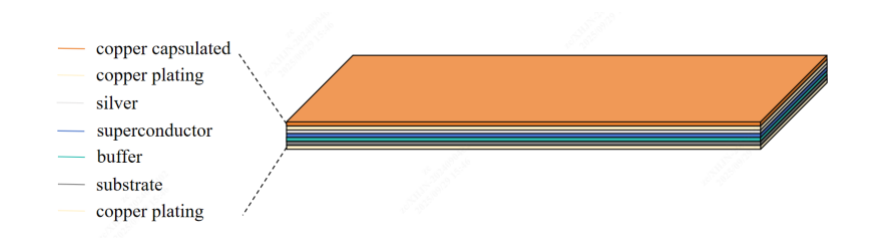


FIG. 4. Schematic diagram of the encapsulated HTS tape structure.

For the assembly method, we use fixtures and torque wrenches for pressure application during the joint formation, rather than conventional soldering irons and manual soldering. This approach ensures precise pressure control and better repeatability, reducing potential process-related issues. The key to achieving a demountable joint lies in the solder selection. We utilize the melting point difference between pure indium (156.6°C) and Sn63Pb37 (183°C). Sn63Pb37 solder is used to encapsulate the HTS tape and copper strip. For joint assembly, pure indium foil is placed between two composite conductors. The assembly is then heated and pressurized using fixtures, causing the indium to melt and form the joint. The complete structure is shown in Figure 5 (four-view drawing).

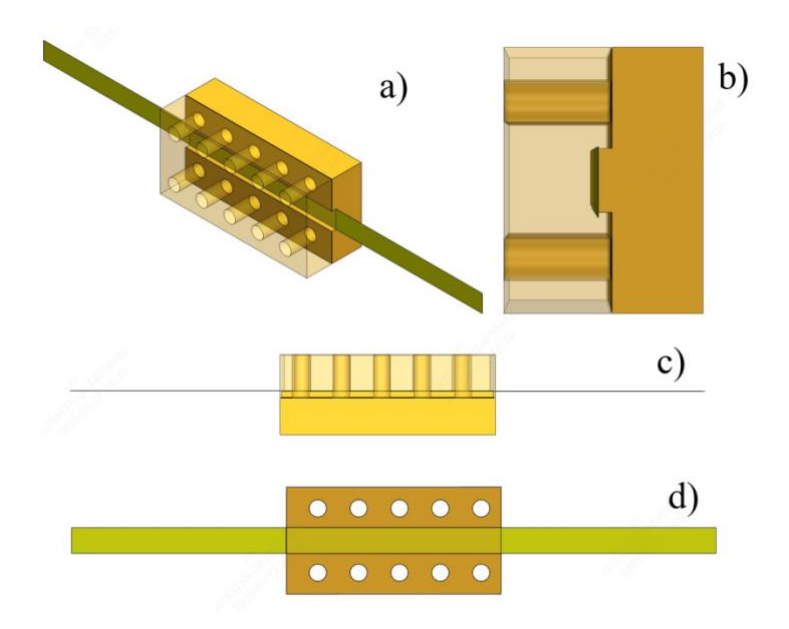


FIG. 5. Detachable joint structure Broussonetia papyrifera four-view diagram: a) Main view; b) Side view; c) Front view; d) Top view

## 2.2. Sample Preparation Process

The sample preparation for demountable joints involves assembly and disassembly processes.

Assembly Process:

Prepare twice the number of single-side copper-clad HTS tapes according to the stacking number, divided into Group A and Group B;

(a) Arrange Group A tapes with superconducting sides facing the same direction. Using one end as a reference, stagger each tape by 10 mm shorter than the one behind it, then secure with polyimide tape (Figure 6). Repeat for Group B;



FIG. 6. Physical diagram of sample assembly process step a.

- (b) Pair Group A and Group B tapes with superconducting faces opposing each other, inserting a 0.1 mm thick pure indium foil between them;
- (c) Wrap the entire joint section with polyimide tape for fixation and insulation between the tapes and pressure blocks (Figure 7);



FIG. 7. Physical diagram of sample assembly process step c.

- (d) Place the joint into the groove of one pressure block (concave block). Align the other pressure block (convex block) and loosely fasten with bolts;
- (e) Insert heating rods and a PT100 temperature sensor into the side holes of the pressure blocks. Control the temperature to 160°C until the indium melts. Tighten with a torque wrench to the appropriate torque, then cool with an air blower. The sample is now prepared.

Disassembly Process:

- (a) Separate the joint from the pressure blocks;
- (b) Replace with two flat pressure blocks, place the joint between them, and press lightly. Heat to 160°C using the same method;
- (c) After the indium melts, insert a blade at one end of the joint to initiate separation, then slide along the joint length to fully separate. Remove the pressure blocks and cool;
- (d) Remove residual indium from both tape groups using a soldering iron. The joint is now ready for reassembly; **Note:** During assembly step c, insulate the pressure blocks with polyimide tape to prevent melted indium from bonding the tapes to the blocks. Ensure the entire joint sits within the groove for proper positioning. In step e, adjust the torque based on the stacking number (refer to Chapter 3). During disassembly step b, using flat blocks facilitates blade insertion for separation.

## 3. THEORETICAL SIMULATION AND ANALYSIS OF DEMOUNTABLE JOINTS

# 3.1. Stress Simulation Model and Boundary Conditions

For modeling, structural optimization was applied by ignoring gaps in the multi-tape lap joint, treating it as a solid tape. This reduces mesh count, computation time, and improves convergence. To verify this simplification, a comparison was made using a two-tape lap joint with and without a 1 mm gap (Figure 8). Results show nearly identical maximum stress values and distributions, with high stress at the edges and near the bolts. Therefore, the simplified gap-free model is acceptable for multi-tape simulations, noting that the modeled tape layers will be one more than the actual stacking number.

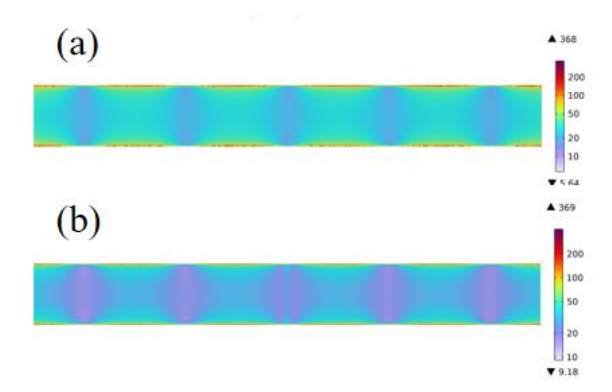


FIG. 8. Stress distribution diagram of two-tape lap joint: (a) Ignoring gap modeling; (b) Not ignoring gap modeling

Boundary conditions included fixed constraints and bolt preloads. The fixed constraint was applied to the bottom surface of the heating copper plate, while bolt preloads were applied to the bolt columns. The tapes were fixed between two copper blocks (Figure 9).

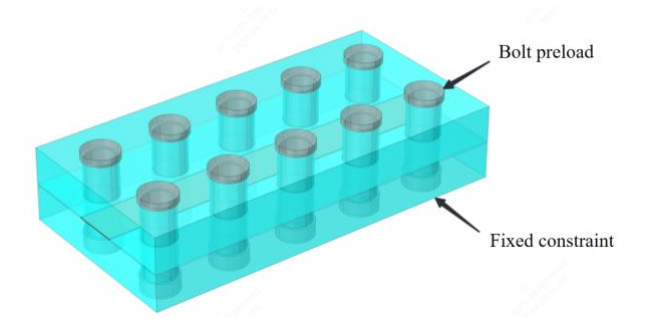


FIG. 9. Stress Simulation Boundary Condition Setup

## 3.2. Joint Resistance Simulation Model and Boundary Conditions

A 3D model of Figure 2 was created in COMSOL with a 1 mm joint gap, using the Electric Currents module. Ignoring the effect of torque on effective contact area, and assuming good contact, a contact resistivity of 40  $n\Omega \cdot cm^2$  was set for all joint interfaces. A 0 V potential was applied at one end and a 1 A current at the other (Figure 10). The average electric potential at the current terminal was calculated to determine resistance.



FIG. 10. Joint resistance Simulation Boundary Condition Setup

## 3.3. Simulation Results and Analysis

Simulations were conducted for various stacking numbers and bolt torques relevant to experimental conditions. Maximum stress values are summarized in Table 2.

TABLE 2. Maximum Stress Simulation Results

Stacking number	10N*m	15N*m	20N*m	25N*m
1 Tape	49 MPa	120 MPa	244 MPa	328 MPa
3 Tapes	50 MPa	157 MPa	284 MPa	368 MPa
5 Tapes	53 MPa	200 MPa	326 MPa	407 MPa
7 Tapes	55 MPa	286 MPa	369 MPa	445 MPa
9 Tapes	60 MPa	311 MPa	401 MPa	489 MPa

Results show that maximum stress increases with bolt torque for all stacking numbers. Under the same torque, higher stacking numbers lead to greater stress. At lower torques (e.g., 10 N·m), the stress increase with stacking number is less pronounced.

The simulated stress is compressive. Based on literature, the maximum allowable compressive stress for HTS tapes is around 400 MPa. Thus, for 5-tape and 7-tape joints, bolt torques above 25 N·m are very risky. For 9-tape joints, the torque should be kept below 20 N·m.

For joint resistance simulation, two studies were conducted:

- Constant joint length, varying stacking number (Figure 11);
- Constant stacking number, varying joint length (Figure 12);

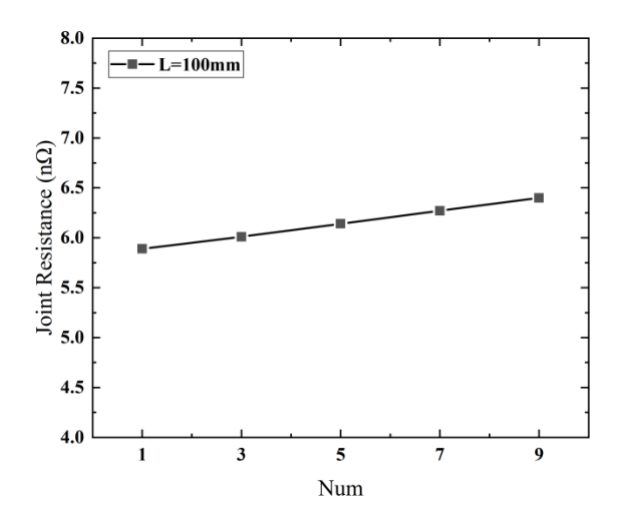


FIG. 11. Simulation Results of the Influence of Conductor number on Resistance

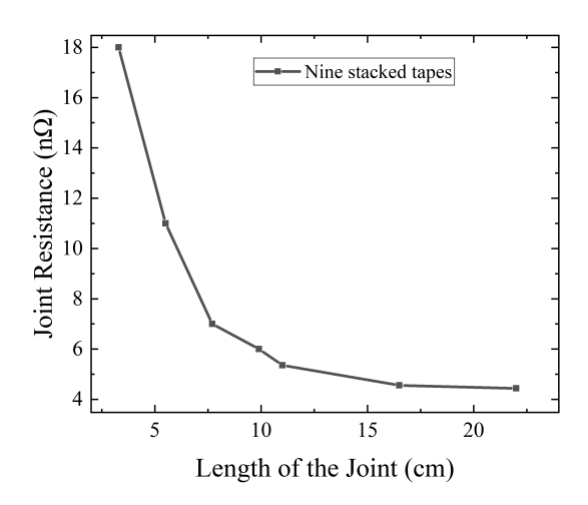


FIG. 12. Simulation Results of the Influence of Joint Length on Resistance

# 4. EXPERIMENTAL TESTING AND VALIDATION OF DEMOUNTABLE JOINTS

# 4.1. Experimental Procedure

The study of demountable joints is divided into two parts: the first part investigates the factors affecting the resistance of demountable joints, and the second part examines the demountability of the joints. For the first part, to study the factors influencing joint resistance, we need to control the variables. There are three variables: joint length L, number of tapes per group Num, and applied bolt torque F. First, with the joint length L kept constant (100 mm) and the applied bolt torque controlled at 10 N·m per bolt, the number of tapes per group Num is gradually increased from a single superconductor tape to 3, 5, 7, and 9 tapes. Then, with the number of tapes per group Num fixed at 9 and the applied bolt torque at 10 N·m, the joint length is varied as 50 mm, 100 mm, and 200 mm. Finally, when investigating the effect of applied bolt torque F on joint resistance, based on the stress simulation results from Chapter 3, the influence of bolt torque on joint resistance should be comprehensively judged in combination with the number of tapes. For the second part, which aims to study the demountability of the joints, we conduct experiments through the following procedure: Before assembling the joint, test the critical current of all high-temperature superconducting tapes. After joint assembly, test the critical current and resistance of the joint, ensuring that the critical current and resistance after the first assembly meet the criteria. Then, disassemble and reassemble the joint, test the critical current and resistance after the second assembly, repeat this process twice, and compare the obtained data from the two reassemblies with the data from the first assembly. If

the critical current shows no attenuation and the joint resistance is below the simulated value, the joint is considered to have demountability.

# 4.2. Testing Method

The standard four-probe method is used. For multi-tape stacked joints, careful design of current and voltage terminals is crucial for uniform current distribution and accurate voltage measurement. Current terminals use a stepped copper block design to ensure current is evenly distributed to each tape (Figure 13). Voltage taps are made by soldering copper pieces to the superconducting side of each tape at the same cross-section, then connecting them together to measure the average potential (Figure 14).

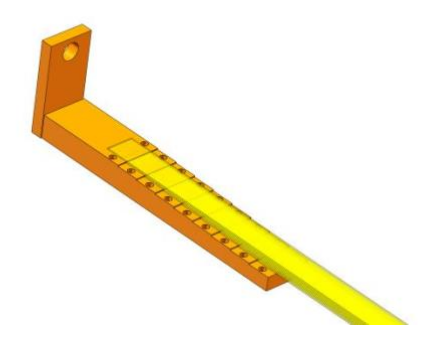


FIG. 13. Three-dimensional diagram of current terminal.

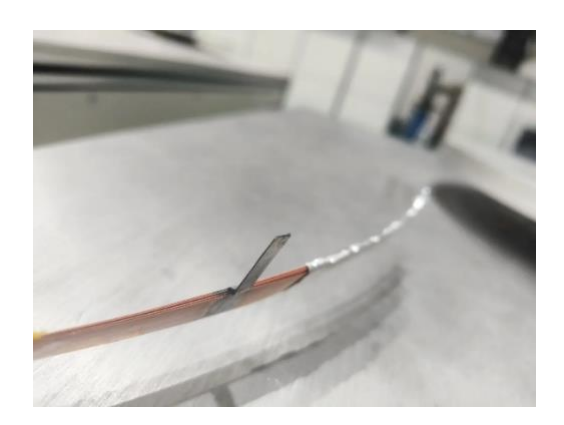


FIG. 14. Physical diagram of voltage taps.

The U-I curve is fitted using the formula:  $U = U_0 + R \times I + E \times L \times (I/Ic)^n$ . Where: U, I = measured voltage and current;  $U_0$  = offset voltage;  $E = 1 \mu V/cm$ ; L = voltage tap distance; n = dimensionless parameter (5–30) representing superconductor characteristics. Using Origin software, Ic and joint resistance R are obtained from the fit.

For multi-tape stacks, the critical current is not simply the sum of individual tape Ics due to magnetic field effects. Field-dependent Ic degradation is acceptable, but degradation from physical damage is not. To distinguish these, the field-dependent Ic degradation for 3, 5, 7, and 9-tape stacks must be known. COMSOL simulation can provide this, but available Jc-B data only includes perpendicular field effects, leading to potential underestimation. Therefore, experimental measurement of the actual critical current for different stack numbers was performed (Figure 15). Given the variation in single-tape Ic (Table 1), if the experimental value exceeds the simulation by no more than 20%, the simulation is considered credible. During joint fabrication, if the measured Ic is not lower than the simulated value, the tape is considered undamaged.



FIG. 15. Physical diagram of critical current testing for stacked superconducting tapes.

## 4.3. Experimental Results and Analysis

First, the critical current ranges for different stack numbers were determined experimentally (Figure 16). Combined with simulations, the Ic criteria are established in Table 3.

TABLE 3. Critical Current Standards for Different Stack Numbers

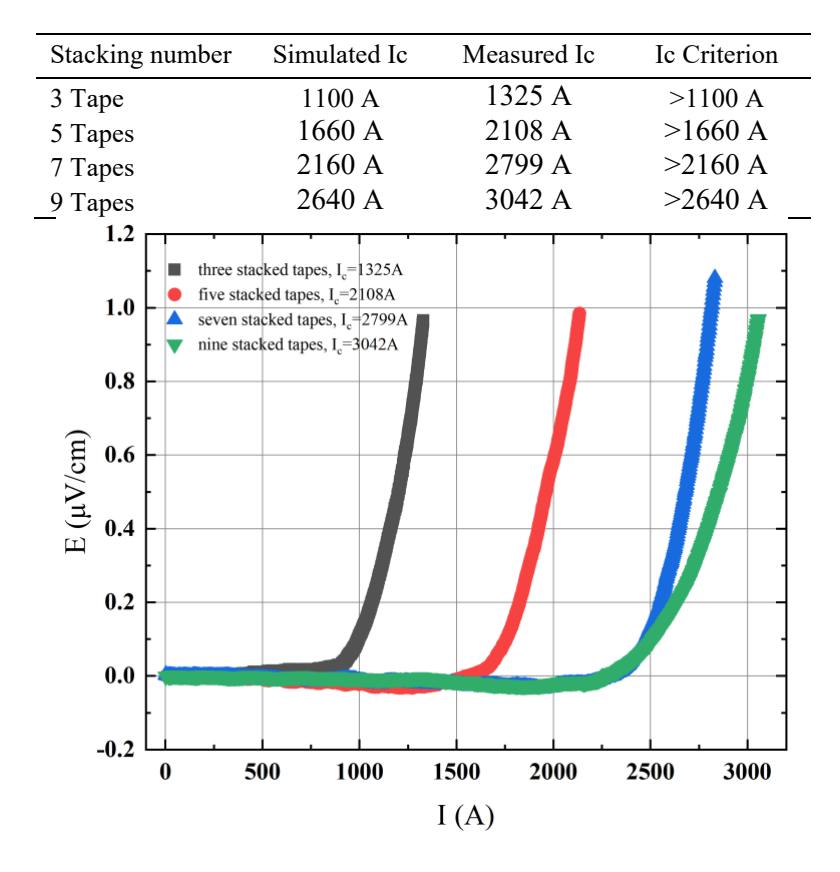


FIG. 16. Results of critical current testing for stacked superconducting tapes.

According to the experimental plan in Section 4.1, we first investigated the factors affecting joint resistance, specifically the influence of the number of tapes Num and joint length L on joint resistance. The experimental results are shown in Figures 17 and 18.

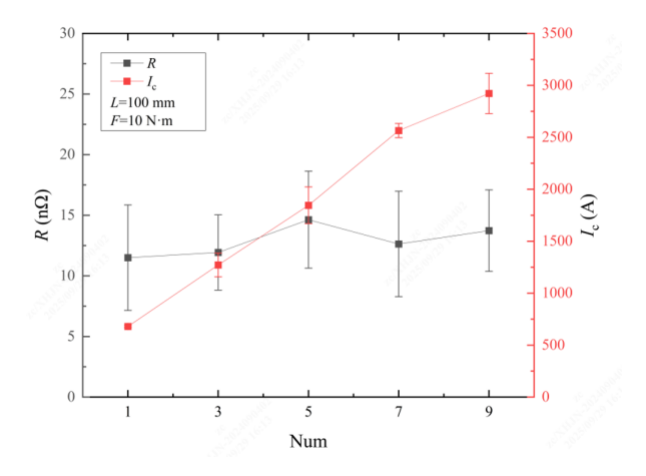


FIG. 17. Test results of the influence of the tape number on resistance.

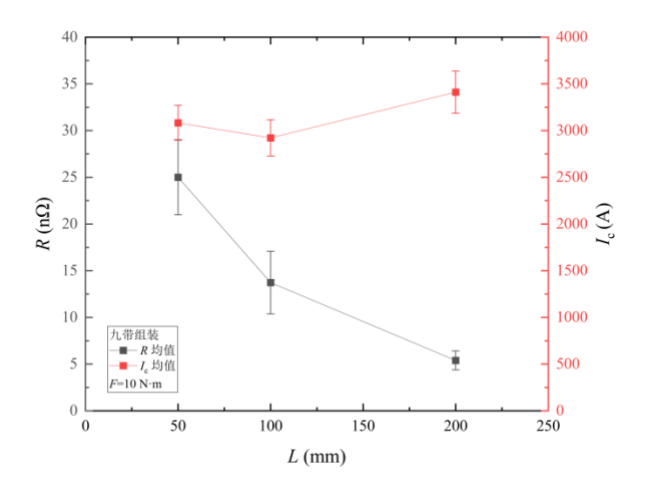


FIG. 18. Test results of the influence of the joint length on resistance.

From the figures, it can be seen that when joint length and applied bolt torque are kept constant, joint resistance has no direct correlation with the number of tapes. However, when the number of tapes and applied bolt torque are kept constant, joint resistance decreases with increasing joint length, showing an inverse relationship. These two conclusions are consistent with the simulation results.

Next, we continued to study the effect of applied bolt torque on resistance, with joint length fixed at 100 mm. The test results are shown in Figures 19 and 20.

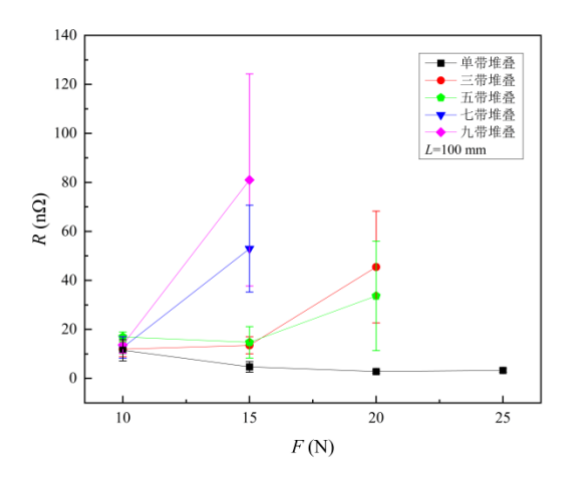


FIG. 19. Effect of Bolt Tightening Torque on Joint Resistance with Varying tape number.

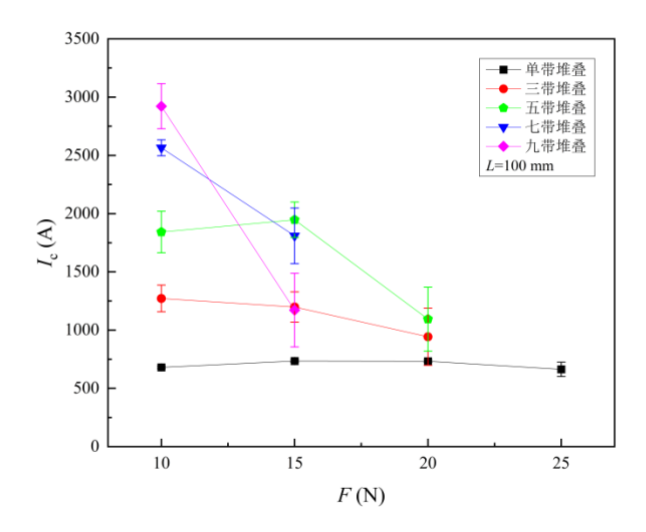


FIG. 20. Effect of Bolt Tightening Torque on Critical Current with Varying tape number.

From the figures, it can be observed that for a single tape, joint resistance decreases with increasing bolt torque up to  $15~\rm N\cdot m$ , after which resistance saturates and hardly decreases further, with no damage occurring throughout the pressure increase process. For three and five tapes, when the bolt torque is less than or equal to  $15~\rm N\cdot m$ , joint resistance remains almost unchanged. However, when the bolt torque exceeds  $15~\rm N\cdot m$ , resistance increases and critical current decreases, indicating that stress concentration has occurred inside the joint, causing local stress to exceed the maximum compressive stress that the tape can withstand. For seven and nine tapes, only bolt torques less than or equal to  $10~\rm N\cdot m$  are safe; torques greater than  $10~\rm N\cdot m$  cause joint damage. Although this conclusion does not exactly match the simulation values, possibly due to some boundary conditions in the simulation not fully aligning with the actual experimental scenario, the trend is consistent: the more tapes there are, the more prone the joint is to stress concentration under the same torque.

Then, we experimentally verified the demountability of the joints. We started with simple single-tape stacked joints to also validate the engineering feasibility of the disassembly process described in Section 2.2. We performed three consecutive assembly and disassembly cycles on a single-tape stacked joint sample with L=100 mm and  $F=25 \text{ N} \cdot \text{m}$ , obtaining three sets of post-assembly joint data as shown in Figure 21.

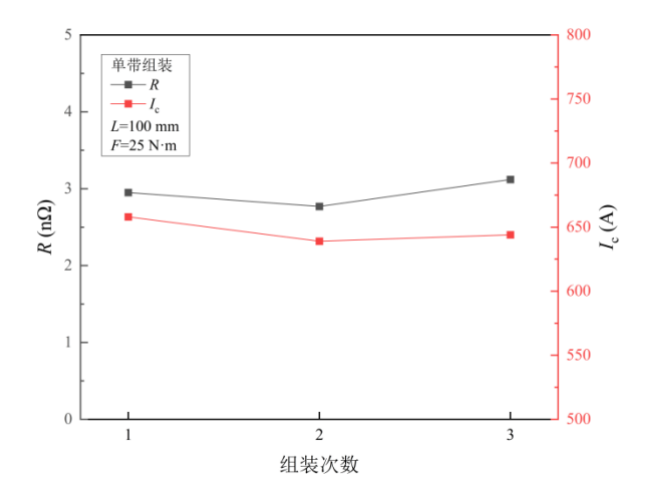


FIG. 21. Test results of single-tape joint after each assembly.

The data show that the critical current of the single-tape stacked joint did not degrade after each disassembly and reassembly, and the variation in joint resistance was less than 1  $n\Omega$ , within the error range. This proves that the disassembly process in Section 2.2 is fundamentally sound and allows for non-destructive disassembly of the joint. However, when applying the same process to nine-tape stacked joints, the difficulty increases significantly because there are height differences between each layer of the joint interface, making it impossible to separate the entire joint directly with a blade after secondary heating. Despite the increased difficulty, with careful operation, it is still possible to achieve layer-by-layer separation and ultimately disassemble the entire joint. We also performed three consecutive assembly and disassembly cycles on a nine-tape stacked joint sample with L=100 mm and F=10 N·m and tested it, with results shown in Figure 22.

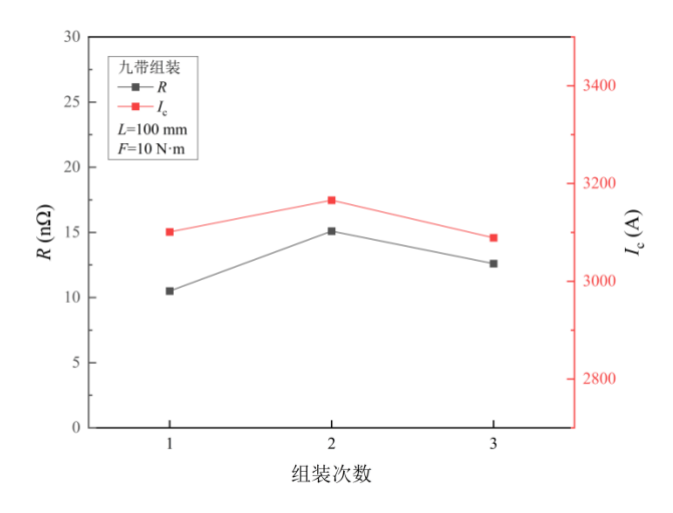


FIG. 22. Test results of nine-tape joint after each assembly.

From the figure, it can be seen that after three disassembly and reassembly cycles, the critical current of the nine-tape stacked joint remains within a reasonable range, above the damage criterion. The variation in joint resistance is slightly larger compared to the single-tape stack, but overall, resistance is influenced by more factors. Therefore, we accept resistance values as long as the maximum does not exceed twice the average. The experimental results for both single and nine-tape joints demonstrate that the joint has strong demountability, providing assurance for future demountable coils.

## 5. CONCLUSION

This paper presents a comprehensive study on the structure, fabrication, simulation, and experimentation of demountable joints—the key challenge for demountable coils. The design starts with a simple lap joint structure, enhanced by encapsulating a copper strip on the superconducting side of the HTS tape for mechanical strength. The melting point difference between indium and Sn63Pb37 solder enables low resistance while ensuring demountability. Simulations and experiments analyzed factors affecting joint resistance and the impact of bolt torque on resistance and critical current. Both confirmed that joint resistance is inversely proportional to length and independent of stack number. They also showed that higher stack numbers are more susceptible to damage under the same torque. Experimentally, for 9-tape lap joints, the maximum safe bolt torque is 10 N·m. However, lower torque may not minimize resistance, indicating a need for future work to balance tape safety and joint quality. Finally, tests on single and nine-tape joints demonstrated successful non-destructive disassembly and highly consistent performance after reassembly. This research provides a solid theoretical foundation for demountable coils, solving a major developmental challenge. However, further work is needed to apply these demountable joints effectively in actual demountable coil systems.

If you need to use subpoints, please use this format:

- First bullet point.
- Section bullet point.
  - First subpoint;
  - Second subpoint.
- Third bullet point.

Please note the punctuation at the end of the points.

#### 5.4. Numbered lists

If you use a numbered list in your paper, please format it as below, noting the punctuation at the end of the points:

- (a) First bullet point.
- (b) Section bullet point.
  - (i) First subpoint;
  - (ii) Second subpoint.
- (c) Third bullet point.

Please use (a), (b), etc., unless your text refers to the points elsewhere as 'the first point', 'the second point' and so on — in this case, please use (1), (2), etc.

## 5.5. General formatting

Only the font Times New Roman should be used in the paper. The font Symbol should never be used in files intended for publication as it is not a Unicode font and letters may change during production (for example,  $\mu$ Sv may print as mSv if the character  $\mu$  is inserted in Symbol font).

Underlining should not be used. Bold and italic may be used for emphasis, but should be used sparingly. Paragraph line spacing is 12 point for 9 point text, 13 point for 10 point text and 14 point for 12 point text, as used in this example paper. Only one space is used following a full stop.

Footnotes<sup>1</sup> should be used only where necessary. They should be inserted at the end of each page, and not at the end of the paper as endnotes.

## **ACKNOWLEDGEMENTS**

The heading of the acknowledgements section is Times New Roman 10 point bold capitals, centred. The acknowledgements section is an optional section and can be used to list funding bodies and other sponsors of the research, and to mention people who supported the research but whose contribution was not of a type to merit authorship of the paper.

# REFERENCES

- [1] AUTHOR, A., Book Title in Title Case, Series No. if applicable, Publisher, Place of Publication (Year).
- [2] AUTHOR, A., Internal Report Title in Title Case, internal report, Organization, Location, Year.
- [3] LETTER-WRITER, A., Organization, personal communication, Year.
- [4] RESEARCHER, A., Organization, unpublished data.
- [5] CHAPTER-AUTHOR, A., "Title of chapter in sentence case", Book Title in Title Case, Publisher, Place of Publication (Year).
- [6] AUTHOR, A., AUTHOR, B., AUTHOR, C., Journal article title in sentence case, Abb. J. Title 1 2 (Year) 120-123.
- [7] AUTHOR, A., Title of Web Page or On-line Database in Title Case (Year),

<sup>&</sup>lt;sup>1</sup> Text in a footnote is Times New Roman 9 point regular.

- www.webpage.com/exact-subpage-being-cited
- [8] AUTHOR, A., "Paper title in sentence case", Conference Title in Title Case (Proc. Int. Conf. Place of Conference, year), Publisher, Place of Publication (Year).
- [9] PRESENTER, A., "Title of presentation in sentence case", Paper No., paper presented at Organization seminar on subject, Location, year.
- [10] Title of INFCIRC in Title Case, INFCIRC No., IAEA, Vienna (Year).

#### **BIBLIOGRAPHY**

AUTHOR, A., Book Title in Title Case, Series No. if applicable, Publisher, Place of Publication (Year).

— Title of Book by Same Author in Title Case, Series No. if applicable, Publisher, Place of Publication (Year).

AUTHOR, A., AUTHOR, B., Book Title in Title Case, Series No. if applicable, Publisher, Place of Publication (Year).

## ORGANIZATION A (Location)

Book Title in Title Case, Series No. if applicable (Year). Book Title in Title Case, Series No. if applicable (Year). Book Title in Title Case, Series No. if applicable (Year).

# ORGANIZATION B (Location)

Book Title in Title Case, Series No. if applicable (Year). Book Title in Title Case, Series No. if applicable (Year). Book Title in Title Case, Series No. if applicable (Year). Book Title in Title Case, Series No. if applicable (Year). Book Title in Title Case, Series No. if applicable (Year).